Applied Physics Letters ARTICLE scitation.org/journal/apl

Investigation of proton irradiation induced E_C-0.9 eV traps in AlGaN/GaN high electron mobility transistors

Cite as: Appl. Phys. Lett. **121**, 092102 (2022); doi: 10.1063/5.0103302
Submitted: 15 June 2022 · Accepted: 27 July 2022 ·
Published Online: 30 August 2022

View Online Export Citation CrossMark

Pengfei Wan,[1] Weiqi Li,[1] Xiaodong Xu,[1] Yadong Wei,[1] Hao Jiang,[1] Jianqun Yang,[1] Guojian Shao,[2] Gang Lin,[2] Chao Peng,[3] Zhangang Zhang,[3] and Xingji Li[1,a)]

AFFILIATIONS

[1]School of Materials Science and Engineering, Harbin Institute of Technology, Harbin 150001, China
[2]Nanjing Electronic Devices Institute, Nanjing 210016, China
[3]Science and Technology on Reliability Physics and Application of Electronic Component Laboratory, China Electronic Product Reliability and Environmental Testing Research Institute, Guangzhou 510000, China

[a)]**Author to whom correspondence should be addressed:** lxj0218@hit.edu.cn

ABSTRACT

Electron traps in AlGaN/GaN high electron mobility transistors were studied by combining theoretical and experimental methods. Energy levels about E_C-0.9 eV due to irradiation are identified by deep-level transient spectroscopy (DLTS). Two electron traps, H1 (E_C-0.63 eV) and H_2 (E_C-0.9 eV), were observed in the DLTS spectra. H1 was produced in device or material manufacturing, and H2 was caused by displacement damage. First, we reported that the signal peak of H2 can contribute from three defects labeled H2-1, H2-2, and H2-3 with energies E_C-0.77 eV, E_C-0.9 eV, and E_C-0.98 eV, respectively. According to defect migration temperature and first principles calculation results, it is found that different configurations of di-nitrogen vacancy structures are the source of E_C-0.77 eV and E_C-0.9 eV signals. The defect of E_C-0.98 eV is more stable at high temperatures, which may be related to gallium vacancy.

Published under an exclusive license by AIP Publishing. https://doi.org/10.1063/5.0103302

Gallium nitride (GaN) is one of the most promising materials for next-generation power and frequency devices used in space[1] because of its high bonding strength, high breakdown electric field, good mobility, and high saturation velocity,[2] which have led to GaN-based power field-effect transistors (FETs) or high electron mobility transistors (HEMTs) with low energy consumption and high irradiation hardness.[3] The performance and reliability of heterojunction FETs and HEMTs have been reported by different groups.[4,5] Point defects and impurities strongly affect the optical and electrical properties of semiconductors. Compared with Si-based devices, the fabrication process and the study of defects in GaN are not mature enough, and the properties of point defects in GaN are not well understood. Understanding the relationship between point defects and energy states in the bandgap and controlling them are critical to the development of high-performance GaN devices. Various point defects are introduced during material growth, device manufacturing, and service.[6] For GaN material and devices, the most common defect with energy level of E_C-0.5–0.6 eV (Refs. 7–9) has been verified to be related to Fe impurity,[10–12] which is considered to relate to gate delay and reduce the frequency characteristics.[13,14] However, the defects of E_C-0.7–1.1 eV usually appear in irradiation samples.[15–20] Our previous research results show that the defect is closely related to the irradiation degradation of device performance, but this defect is still not well known.[21,22] The EE2 peak (E_C-0.98 eV) was found in electron irradiated GaN samples.[20] The signal was identified as nitrogen interstitial by deep-level transient spectroscopy (DLTS) test. In this study, combining theoretical and experimental results, we found that the DLTS signal with an energy level of E_C-0.7–1.1 eV originates from multiple defects. Di-vacancies of nitrogen with different configurations may be one of the components of this signal.

The device was grown on a 4H-SiC substrate by metalorganic chemical vapor deposition (MOCVD). The device consisted of a 2-μm-thick GaN layer and a 25-nm AlGaN layer. The gate–drain and gate–source spacings were 2.95 and 0.8-μm, respectively, and the gate length was 0.25-μm. The chip thickness was 80-μm. The passivation layer was Si_3N_4 and the Al composition was 25%. A Ti/Al/Pt/Au structure was used to form the source/drain Ohmic electrodes and Ni/Au structure was used as the Schottky gate. The device was composed of

Published under an exclusive license by AIP Publishing

ten fingers with a gate width of 1.25 mm. 3 MeV Proton irradiation was performed in the fluence of 3×10^{13}, 7×10^{13}, and 1.2×10^{14} cm^{-2} at room temperature, where samples were grounded during experiments. The annealing test is used to study defect characteristics after irradiation. According to migration barrier of defects, the samples were annealed twice at 520 K for 3 h each time. The transfer characteristics of the samples were recorded during irradiation and annealing. Temperature-scan DLTS was performed first, where the maximum measurement temperature was limited to 390 K. This temperature limitation prevents the migration of defects and enables the samples to be characterized in the irradiated state. Isothermal current transient spectroscopy (ICTS) measurements and multi-exponential analysis were performed at 340–360 K, which were used to evaluate the overlap defect signal and the amplitude of the transient signal.[23,24] The electrical performance was tested with a Keithley 4200SCS. DLTS measurements for traps were performed using a PhysTech HERA FT 1030 instrument in conjunction with a I–V meter. Voltage pulses with $V_R = -(2.5 - {}_{\Delta}V_{TH})$, $V_P = -7$ V, and pulse width of 1 ms to the gate of the device at $V_{DS} = 1$ V. The defect detection area is mainly in the GaN layer below the gate by analyzing the electric field distribution using the TCAD (Technology Computer Aided Design). Annealing was carried out in a high temperature annealing furnace.

Figure 1 shows the transfer characteristic, threshold voltage, and transconductance of AlGaN/GaN HEMTs during irradiation and annealing. The threshold voltage of the samples positive shift after irradiated by 3 MeV proton, and there is a linear relationship between fluence vs value of threshold voltage shift. Maximum transconductance of devices decrease after irradiation, which means there is a decrease in the carrier mobility. High-energy protons penetrate heterojunction and produce displacement defects in semiconductors. During annealing, the threshold voltage continues to negative shift and the carrier mobility continues to decrease, which caused by defect evolution. At present, it is generally believed that the negatively charged defects produced by irradiation caused this phenomenon.[4] By contrast, positively charged defects lead to negative shift of the threshold voltage. The charged defects caused by irradiation are effective scattering center, which lead to the decrease in the carrier mobility. The change in mobility during annealing is most likely caused by the evolution of neutral defects into charged defects. After annealing at 520 K for 3 h, the change in transconductance and threshold voltage in irradiated samples both reached saturation. This means that there is a defect evolution during annealing and in the end at this temperature after 3 h.

As shown in Fig. 2, two peaks, H1 and H2, were found in the DLTS spectra. The energy levels of the defects were obtained by testing the DLTS spectra at different Tw's and performing an Arrhenius fit using the Box-car method.[23] The energy levels of H1 and H2 peaks are $\sim E_C$-0.63 eV and $\sim E_C$-0.9 eV. The H1 peak also showed in the unirradiated samples indicates that the defect of H1 is produced in the device or material manufacturing. The signal height of H1 remains almost unchanged after irradiation but decreases after annealing. While the H2 peak appears after irradiation and the signal height is related to fluence. After annealing, the signal height of the H2 peak is reduced and 3 h of annealing is enough to saturate the reduction in the H2 peak. Changes in the H2 defect signal during irradiation and annealing coincide with the changes in the device threshold voltage. This means that the H2 defect is one of the significant causes of device performance degradation. Moreover, signal saturation in annealing indicates that the H2 is an overlapped signal which contains more than one defect. Some of the defects disappeared during annealing at 520 K, but thermal stability defects are retained.

ICTS and multi-exponential analysis[24] were used to distinguish the different defect energy levels. As shown in Fig. 3, three different energy levels exhibiting different time constants at the same temperature were discovered with the energy levels E_C-0.77 eV, E_C-0.9 eV, and E_C-0.98 eV. A comparison of these three defects before and after annealing is shown in Table I. The amplitudes of the current transient of E_C-0.77 eV and E_C-0.9 eV decrease, while the intensity of E_C-0.98 eV almost remain unchanged after annealing. A similar conclusion was obtained during defect detection and suggests that the defect is nitrogen interstitial.[20] However, if H2 only consist of nitrogen interstitial in this work, the H2 peak will disappear at 520 K instead of saturating. As we discussed above, the H2 peak in DLTS spectra is an overlapped signal.

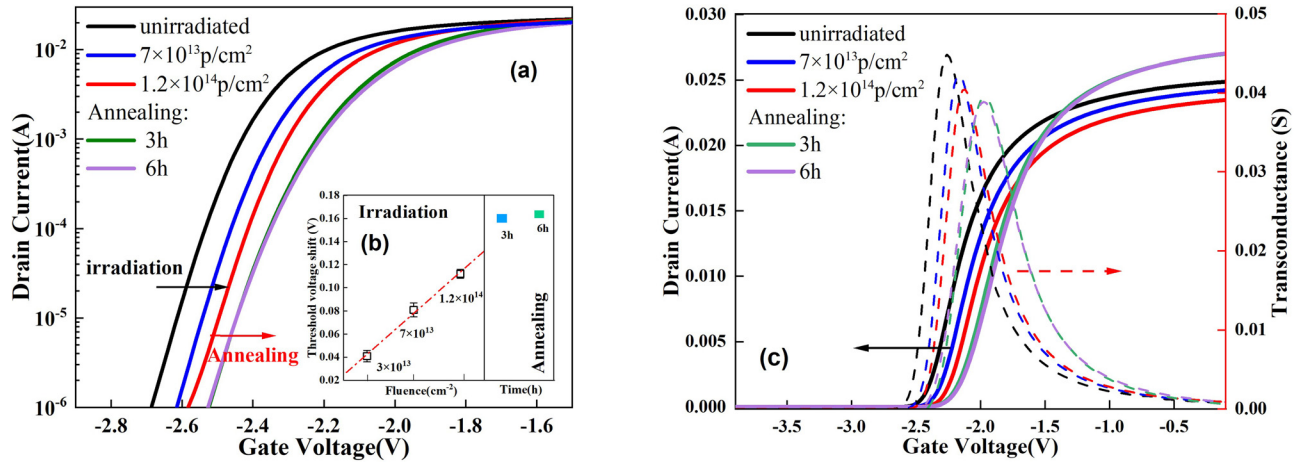

FIG. 1. (a) Transfer characteristic in a log scale, (b) the shift of threshold voltage, and (c) transfer characteristic and transconductance in a liner scale of AlGaN/GaN HEMTs during irradiation and 520 K annealing.

Published under an exclusive license by AIP Publishing

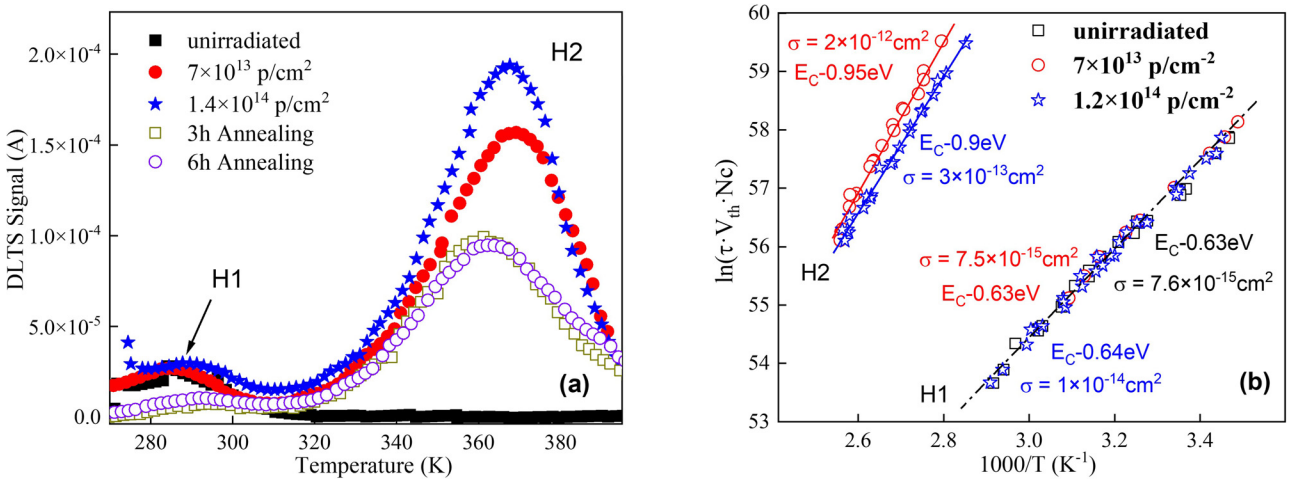

FIG. 2. (a) DLTS spectra for irradiated and annealing samples at $T_W = 1$ s and (b) Arrhenius plots of $\ln(\tau \cdot V_{th} \cdot N_C)$ vs 1000/T for electron trap levels H1 and H2 observed in the DLTS spectra after proton irradiation. The Arrhenius plots were obtained from the Box-car method.

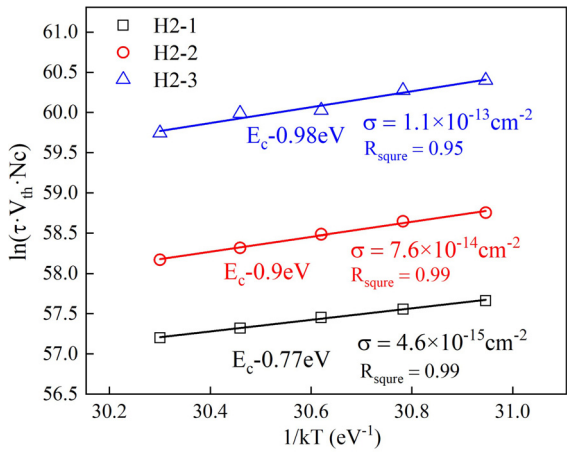

FIG. 3. Arrhenius plots of $\ln(\tau \cdot V_{th} \cdot N_C)$ vs 1/kT for electron trap levels (k is the Boltzmann constant). The Arrhenius plots were obtained from ICTS and multi-exponential analysis.

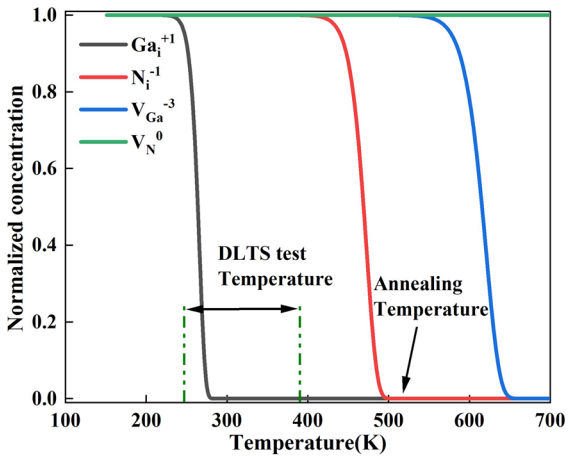

FIG. 4. The normalized concentration vs temperature of Ga_i^{+1}, N_i^{-1}, V_{Ga}^{-3}, and V_N^0 in 3 h.

TABLE I. The fitted values (in eV) for the trap levels, amplitudes (in mA) of current transient, and time constants (in s). Analyses were performed at 340–360 K, and the amplitudes were obtained at 360 K.

Transition level	Time constants	Amp after irradiation	Amp after 6 h annealing
E_C-0.77	0.1–0.01	0.264	0.034
E_C-0.9	0.1–1	0.776	0.045
E_C-0.98	1	0.036	0.03

The recombination of the point defect in semiconductors during annealing is related to the diffusion barrier and annealing temperature. The relationship between normalized concentration of defects and temperature in GaN is shown in Fig. 4. The heterojunction in AlGaN/GaN HEMTs is usually made of unintentional doping n-type material. The samples in this experiment are also unintentional doping n-type. Therefore, we only consider the migration barrier of the defects with most stable charge state when Fermi level nears the conduction band. The charged states and diffusion barriers are obtained from formation energy and transition level, which is predicted by Van de Walle *et al.*[25] Gallium interstitial shows a rather low diffusion temperature, which will move and recombine with other defects under room temperature. The diffusion temperatures of the gallium and nitrogen vacancies are higher than the annealing temperatures in this study. Diffusion temperature of nitrogen interstitial is higher than the DLTS test temperature and lower than the annealing temperature. Therefore, only the nitrogen interstitial will move in the 520 K annealing. We infer that the reduced DLTS signal during annealing is caused by the recombination of N_i and V_N related defects. The transition level of Ni (0/−1) is

Published under an exclusive license by AIP Publishing

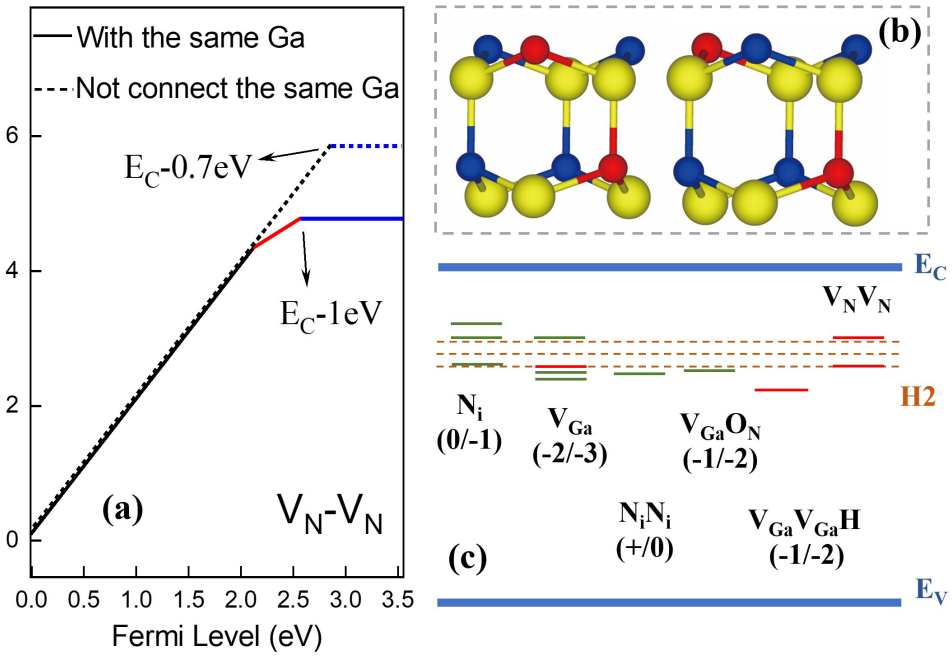

FIG. 5. (a) Formation energy and transition levels of V_N–V_N structures including two V_N connected and not with one Ga. (b) The structure of two V_N–V_N. The red, yellow, and blue balls are the position of V_N, Ga, and N, respectively. (c) Transition levels of defects in gallium nitride. The brown lines are the transition levels of E_C-0.77 eV, E_C-0.9 eV, and E_C-0.98 eV. The red lines are the calculation results in this work and the green lines are references to the published results [N_i (0/−1),[26,27,29] V_{Ga} (−2/−3),[26,27,29] $V_{Ga}O_N$ (−1/−2),[30] N_iN_i (+1/0)[26]].

also around E_C-0.6–1 eV which is similar to the H2 peak [0.6,[26] 0.7,[27] 1,[28,29] and all references which used the HSE (hybrid functional of Heyd, Scuseria, and Ernzerhof) method].

Based on the experimental results, these defects related to the H2 peak may be associated with nitrogen defects. In the present study, we calculated the transition levels and formation energies of the di-vacancy of nitrogen using the first principles method. The results are shown in Fig. 5(a). The calculations were carried out using the projector augmented wave (PAW) method implemented in the VASP code. The HSE06 was chosen during calculation, which considered more accurate compared with experiments.[29] Two configurations of V_N–V_N were considered in Fig. 5(b). The transition levels of V_N–V_N with different structures are E_C-0.7 eV and E_C-1 eV. The value is close to H2–1 and H2–2 in DLTS. Moreover, the formation energy of V_N–V_N is similar with N_i in $E_f = 3.5$ eV and it may be formed in a large quantity under the radiation environment. N_i recombination with V_N–V_N leads to the decrease in H2–1 and H2–2. The possible thermodynamic transition levels calculated by this work and predicted from references are shown in Fig. 5(c) and Table II. In addition to the N_i, the transition level of N_i–N_i (+/0) is also close to H2. The transition levels of V_{Ga} (−2/−3), $V_{Ga}O_N$ (−1/−2), and V_{Ga}–V_{Ga}–H (−1/−2) also close to H2. These V_{Ga} related defect structures are relatively stable at high temperature,[30] and most of them are occupied by additional electrons. These defects can exist at higher temperatures (H2–3) and are the cause of the positive shift of the threshold voltage.

TABLE II. Thermodynamic transition levels of defects predicted by HSE (Hybrid functional of Heyd, Scuseria, and Ernzerhof) and GGA (Generalized Gradient Approximation) with the reference to the conduction-band minimum (CBM).

	Present work	HSE	GGA
N_i (0/−)		0.6[26] 0.7[27] 1[29]	1.5[25,26]
V_{Ga} (−2/−3)	0.9	1.1[26] 1.1[27] 0.7[29]	2.3[25]
N_i–N_i (+/0)		1.1[26]	
V_{Ga}–O_N (−/−2)		1.02[30]	
V_N–V_N (+2/0)	0.7		
V_N–V_N (+1/0)	1	0.9[28]	1[28]

In conclusion, we investigated the irradiation trap in AlGaN/GaN HEMTs using DLTS and first principles method. Two electron trap levels, H1 (E_C-0.63 eV) and H2 (E_C-0.98 eV), were observed in DLTS spectra. The H2 peak contains not only one defect but also an overlapped signal. Three different transition levels are obtained by a multi-exponential fitting method. These energy levels values are E_C-0.77 eV, E_C-0.9 eV, and E_C-0.98 eV, respectively, wherein the amplitudes of E_C-0.77 eV and E_C-0.9 eV will obviously disappear during 520 K annealing in 3 h and saturated, while no annealing was found in the E_C-0.98 eV signal. The disappearance of these signals is attributed to nitrogen interstitial migration and recombines with other defects because only nitrogen interstitial will diffuse from 400 to 520 K in this study. Through the first principles calculation of the defect structure, the V_N–V_N structure is considered to be one of the components of the H2 peak. The recombination of Ni and V_N–V_N leads to the decrease in transient amplitude of E_C-0.77 eV and E_C-0.9 eV. Defect with transition level of E_C-0.98 eV is more high temperature stability, which may have some defects structure related to gallium vacancy.

This work was supported by the Foundation of Science and Technology on Reliability Physics and Application of Electronic Component Laboratory, China Electronic Product Reliability and Environmental Testing Research Institute (No. 6142806200102) and Open Projects of State Key Laboratory of Intense Pulsed Radiation Simulation and Effect, Xi'an, China (No. SKLIPR2020).

Published under an exclusive license by AIP Publishing

AUTHOR DECLARATIONS

Conflict of Interest

The authors have no conflicts to disclose.

Author Contributions

Pengfei Wan: Writing – original draft (lead). **Zhangang Zhang:** Resources (equal). **Xingji Li:** Project administration (equal); Supervision (equal). **Weiqi Li:** Writing – review and editing (equal). **Xiaodong Xu:** Software (supporting). **Yadong Wei:** Software (supporting). **Hao Jiang:** Data curation (supporting). **Jianqun Yang:** Project administration (equal). **Guojian Shao:** Resources (equal). **Gang Lin:** Resources (equal). **Chao Peng:** Resources (equal).

DATA AVAILABILITY

The data that support the findings of this study are available from the corresponding author upon reasonable request.

REFERENCES

[1]M. Carbone, K. Hirche, S. Morand, M. Marin, S. Prevo, A. Guidoin, N. Neugnot, M. G. Alonso, M. R. Álvarez, F. J. P. Marin, E. P. Lapeña, and F. Gómez-Carpintero, in *European Space Power Conference* (IEEE, Juan-les-Pins, France, 2019).

[2]R. Fornari, *Single Crystals of Electronic Materials* (Woodhead Publishing, 2018), p. 351.

[3]Y. Kobayashi and S. Kawasaki, IEEE Trans. Aerosp. Electron. Syst. **52**, 1340 (2016).

[4]S. J. Pearton, F. Ren, E. Patrick, M. E. Law, and A. Y. Polyakov, ECS J. Solid State Sci. Technol. **5**, Q35 (2015).

[5]D. M. Fleetwood, E. X. Zhang, R. D. Schrimpf, and S. T. Pantelides, IEEE Trans. Nucl. Sci. **69**, 1105 (2022).

[6]R. Jiang, X. Shen, J. Fang, P. Wang, E. X. Zhang, J. Chen, D. M. Fleetwood, R. D. Schrimpf, S. W. Kaun, E. C. H. Kyle, J. S. Speck, and S. T. Pantelides, IEEE Trans. Device Mater. Reliab. **18**, 364 (2018).

[7]A. Cavallini, G. Verzellesi, A. F. Basile, C. Canali, A. Castaldini, and E. Zanoni, J. Appl. Phys. **94**, 5297 (2003).

[8]T. Mizutani, T. Okino, K. Kawada, Y. Ohno, S. Kishimoto, and K. Maezawa, Phys. Status Solidi A **200**, 195 (2003).

[9]S. Chen, U. Honda, T. Shibata, T. Matsumura, Y. Tokuda, K. Ishikawa, M. Hori, H. Ueda, T. Uesugi, and T. Kachi, J. Appl. Phys. **112**, 053513 (2012).

[10]M. Silvestri, M. J. Uren, and M. Kuball, Appl. Phys. Lett. **102**, 073501 (2013).

[11]J. Joh and J. A. del Alamo, IEEE Trans. Electron Devices **58**, 132 (2011).

[12]Y. Zhang, Z. Chen, W. Li, H. Lee, M. R. Karim, A. R. Arehart, S. A. Ringel, S. Rajan, and H. Zhao, J. Appl. Phys. **127**, 215707 (2020).

[13]A. R. Arehart, A. Sasikumar, S. Rajan, G. D. Via, B. Poling, B. Winningham, E. R. Heller, D. Brown, Y. Pei, F. Recht, U. K. Mishra, and S. A. Ringel, Solid-State Electron. **80**, 19 (2013).

[14]M. Kuball, M. Ťapajna, R. J. T. Simms, M. Faqir, and U. K. Mishra, Microelectron. Reliab. **51**, 195 (2011).

[15]Z. Q. Fang, G. C. Farlow, B. Claflin, D. C. Look, and D. S. Green, J. Appl. Phys. **105**, 123704 (2009).

[16]Z. Zhang, A. R. Arehart, E. Cinkilic, J. Chen, E. X. Zhang, D. M. Fleetwood, R. D. Schrimpf, B. McSkimming, J. S. Speck, and S. A. Ringel, Appl. Phys. Lett. **103**, 042102 (2013).

[17]S. A. Goodman, F. D. Auret, F. K. Koschnick, J. M. Spaeth, B. Beaumont, and P. Gibart, MRS Internet J. Nitride Semicond. Res. **4**, 606 (1999).

[18]Z. Zhang, E. Farzana, W. Y. Sun, J. Chen, E. X. Zhang, D. M. Fleetwood, R. D. Schrimpf, B. McSkimming, E. C. H. Kyle, J. S. Speck, A. R. Arehart, and S. A. Ringel, J. Appl. Phys. **118**, 155701 (2015).

[19]T. Tanaka, K. Shiojima, T. Mishima, and Y. Tokuda, Jpn. J. Appl. Phys., Part 1 **55**, 061101 (2016).

[20]M. Horita, T. Narita, T. Kachi, and J. Suda, Appl. Phys. Lett. **118**, 012106 (2021).

[21]P. Wan, J. Yang, G. Lv, L. Lv, S. Dong, W. Li, X. Xu, C. Peng, Z. Zhang, and X. Li, IEEE Trans. Nucl. Sci. **68**, 1258 (2021).

[22]P. Wan, J. Yang, H. Lv, E. Guan, H. Li, L. Lv, X. Xu, Y. Wei, Y. Song, W. Li, and X. Li, IEEE Trans. Nucl. Sci. **69**, 1120 (2022).

[23]D. V. Lang, J. Appl. Phys. **45**, 3023 (1974).

[24]A. Scotti, W. Liu, J. S. Hyatt, E. S. Herman, H. S. Choi, J. W. Kim, L. A. Lyon, U. Gasser, and A. Fernandez-Nieves, J. Chem. Phys. **142**, 234905 (2015).

[25]S. Limpijumnong and C. Van de Walle, Phys. Rev. B **69**, 035207 (2004).

[26]I. Diallo and D. Demchenko, Phys. Rev. A **6**, 064002 (2016).

[27]A. Kyrtsos, M. Matsubara, and E. Bellotti, Phys. Rev. B **93**, 245201 (2016).

[28]H. Li, M. Huang, and S. Chen, J. Semicond. **41**, 032104 (2020).

[29]L. J. Lyons and C. G. V. de Walle, npj Comput. Mater. **3**, 12 (2017).

[30]H. Huang, X. Yang, S. Wu, J. Shen, X. He, L. Wei, D. Liu, F. Xu, N. Tang, X. Wang, W. Ge, and B. Shen, Appl. Phys. Lett. **117**, 112103 (2020).

Published under an exclusive license by AIP Publishing